Optimal preparation of high-entropy boride-silicon carbide ceramics

Yan Zhang
Guangdong University of Technology
Shi-Kuan Sun
The University of Sheffield
Wei-Ming Guo (guo1237@126.com)
Guangdong University of Technology
Liang Xu
Guangdong University of Technology
Wei Zhang
Guangdong University of Technology
Hua-Tay Lin (huataylin@comcast.net)
Guangdong University of Technology

Rapid Communication

Keywords: High-entropy boride-silicon ceramics, Borothermal reduction, Boro/carbothermal reduction, Microstructure, Mechanical properties

Posted Date: August 31st, 2020

DOI: https://doi.org/10.21203/rs.3.rs-33290/v3

Version of Record: A version of this preprint was published at Journal of Advanced Ceramics on October 21st, 2020. See the published version at https://doi.org/10.1007/s40145-020-0418-1.

Abstract

High-entropy boride-silicon carbide (HEB-SiC) ceramics were fabricated by using boride-based powders prepared from borothermal and boro/carbothermal reduction methods. The effects of processing routes (borothermal reduction and boro/carbothermal reduction) of HEB powders were examined. HEB-SiC ceramics with nearly relatively full density (>98%) were prepared by spark plasma sintering at 2000 °C. It was demonstrated that the addition of SiC led to slightly coarsening of the microstructure. The HEB-SiC ceramics prepared from boro/carbothermal reduction powders showed the fine-grained microstructure and higher Vickers' hardness but lower fracture toughness values as compared with the same composition prepared from borothermal reduction powders. These results indicated that the selection of the powder processing method and the addition of SiC phase could contribute to the optimal preparation of high-entropy boride-based ceramics.

1. Introduction

In recent years, high-entropy ultra-high temperature boride (HEB) ceramics have been extensively studied by combining the concepts of ultra-high temperature boride ceramic (UHTC) and high-entropy materials [1-3]. HEB ceramics were found to exhibit high hardness and superior oxidation resistance [4-6]. Accordingly, HEB ceramics are considered to possess potential for the broad application [4]. However, HEB ceramics suffered from the difficulty in densification mainly due to the strong covalent bonds and low diffusion rate during the sintering process, as previously observed in traditional UHTC boride systems (e.g. ZrB_2 and HfB_2) [4,5,7,8]. Gild *et al.* [4] fabricated high-entropy boride ceramics by the combination of high-energy ball milling of the precursors and subsequent spark plasma sintering (SPS) at 2000°C. The as-sintered materials exhibited relatively higher hardness (21.0~22.5 GPa) and better oxidation resistance as compared to traditional boride ceramics. However, the relative density reported was only 92.4% due to the contamination of the powder during the milling procedure. The particle size and purity of powder were effectively improved by borothermal reduction and boro/carbothermal reduction, promoting sintering densification [9,10]. Our recent works reported that HEB ceramics could reach higher relative densities of 95.0~99.2% by sintering the HEB powder derived from borothermal reduction and 96.3~98.5% from boro/carbothermal reduction, respectively [11,12]. It was shown that HEB material with nearly full densification (RD=99.2%) and remarkable hardness (28.3±1.6 GPa) could be achieved in the system of $(Hf_{0.2}Zr_{0.2}Ta_{0.2}Cr_{0.2}Ti_{0.2})B_2$ [13].

By reviewing the developmental progress of ultra-high temperature boride ceramics, SiC was added as a secondary phase into the ZrB_2 and HfB_2 system to reduce the sintering temperature and suppress the abnormal grain growth due to the pinning effect. Owing to the toughening effects resulting from the crack deflection and crack bifurcation, the fracture toughness of ZrB_2-SiC and HfB_2-SiC ceramics could be improved [13-15]. A few studies have been performed investigating the addition of SiC into HEB ceramics systems. In a recent study, $B_4(HfMo_2TaTi)C$-SiC_w showed an extremely high Vickers' hardness (35.4 GPa) and excellent oxidation resistance [16]. The introduction of SiC to the HEB ceramic system was reported to improve the densification behaviour as well as mechanical properties [17]. $(Ti_{0.2}Zr_{0.2}Hf_{0.2}Nb_{0.2}Ta_{0.2})B_2$-SiC was fabricated with high density (>97%) by SPS at 1900°C, and the fracture toughness was increased by more than 30% [17]. Recently, Liu *et al.* reported the addition of 20 vol.% SiC into $(Ti_{0.2}Zr_{0.2}Hf_{0.2}Nb_{0.2}Ta_{0.2})B_2$ high entropy ceramics prepared by hot pressing sintering at 1800°C, improving the four-point flexural strength, fracture toughness, and hardness $Hv_{0.2}$ from 339±17 MPa, 3.81±0.40 MPa·$m^{1/2}$, and 23.7±0.7 GPa to 447±45 MPa, 4.85±0.33 MPa·$m^{1/2}$, and 24.8±1.2 GPa, respectively [18]. Nevertheless, more studies

on HEB-SiC ceramic system would be still required to understand the effects of the powder processing methods and the addition of SiC on the densification behaviour and mechanical properties of HEB-SiC ceramics.

In this work, the self-synthesised HEB powders were mixed with SiC particles and sintered by SPS. In particular, two processing methods were examined comparing HEB powders prepared by borothermal reduction and boro/carbothermal reduction. The HEB ceramic systems, namely $(Hf_{0.2}Zr_{0.2}Mo_{0.2}Nb_{0.2}Ti_{0.2})B_2$ and $(Hf_{0.2}Mo_{0.2}Ta_{0.2}Nb_{0.2}Ti_{0.2})B_2$, were chosen in line with our previous studies [11,12]. The influence of the powder-processing routes on the phase assemblage, microstructure, and mechanical properties of HEB-SiC ceramics were emphatically investigated in this study.

2. Experimental Procedure

The starting materials used in this study were HfO_2 (~0.3 μm, purity ≥ 99.95%, Beijing Founde Star Sci. & Tech. Co., Ltd, China), ZrO_2 (~0.6 μm, ≥ 99.8%, Changsha Xili Nanometer Lapping Tech. Co., Ltd, China), Nb_2O_5 (~2.0 μm, ≥ 99.95%, Beijing Founde Star Sci. & Tech. Co, Ltd, China), TiO_2 (~21 nm, ≥ 99.9%, Xuancheng Jingrui New Material Co., Ltd, China), Ta_2O_5 (~0.5 μm, ≥ 99.95%, Zhuzhou Cemented Carbide Group Co., Ltd, China), MoO_3 (~1.0 μm, ≥ 99.9%, Shanghai Naiou Nano Tech. Co., Ltd, China), boron (~1 μm, > 95.60%, Dandong Chemical Engineering Institute Co., Ltd, Dandong China), B_4C (~1.5 μm, ≥ 99.9%, Mudanjiang Diamond Boron Carbide Co. Ltd, China), and graphite (~2.0 μm, ≥ 99.9%, Shanghai Colloid Chemical Co., Ltd, China). The appropriate amount of the raw powders was batched and mixed by roller milling (J_M-6, Xiangtan Sanxing Instrument Co. LTD, China) in ethanol for 24 hours to target the fabrication of $(Hf_{0.2}Zr_{0.2}Mo_{0.2}Nb_{0.2}Ti_{0.2})B_2$ and $(Hf_{0.2}Mo_{0.2}Ta_{0.2}Nb_{0.2}Ti_{0.2})B_2$. Borothermal reduction (utilising mixed oxides and boron) and boro/carbothermal reduction (utilising mixed oxides, boron carbide and graphite) were separately employed to prepare HEB powders by heat-treating the pre-mixed powders at 1600^oC for 1 h under vacuum. The phase fractions obtained by borothermal reduction was calculated as follows: HEB phase = 86.8 wt.%, ZrB_2 = 5.5 wt.%, m-$(Zr,Hf)O_2$ = 5.3 wt.%, t-ZrO_2 = 2.4 wt.% for $(Hf_{0.2}Zr_{0.2}Mo_{0.2}Nb_{0.2}Ti_{0.2})B_2$ and HEB = 97.3 wt.%, m-HfO_2 = 2.7 wt.% for $(Hf_{0.2}Mo_{0.2}Ta_{0.2}Nb_{0.2}Ti_{0.2})B_2$, respectively [11]. For the boro/carbothermal reduction route [12], they were consisted of HEB phase (94.0 wt.%), m-HfO_2 (4.1 wt.%), t-HfO_2 (1.9 wt.%) for $(Hf_{0.2}Zr_{0.2}Mo_{0.2}Nb_{0.2}Ti_{0.2})B_2$ product and HEB (90.4 wt.%), m-HfO_2 (9.0 wt.%), t-HfO_2 (0.6 wt.%) for $(Hf_{0.2}Mo_{0.2}Ta_{0.2}Nb_{0.2}Ti_{0.2})B_2$. More details on the purity and particle size on HEB powders synthesized could be found in Refs. [11] and [12]. 20 vol.% SiC (~0.3μm, ≥ 99.9%, Shanghai Xiangtian New-Materials Co., Ltd, China) was mixed with the as-obtained HEB powders by roller milling (J_M-6, Xiangtan Sanxing Instrument Co. LTD, China) in ethanol for 24 hours using silicon nitride milling media and acetone, and sintered by spark plasma sintering (H-HPD 10-FL, FCT System Gmbh, Germany) at 2000^oC in argon atmosphere for 10 min with a ramping rate of 150 ^oC/min under uniaxial pressure of 30 MPa, (the same process parameters as the HEB ceramics without SiC additive [11,12]). Considering the limited milling media wear and mild milling conditions, it was hypothesised that the purity and particle size of the roller milled samples should have little variation, as compared to those starting from HEB powder without SiC additive in our previous work [11,12]. SiC addition with 20 vol.% fraction was chosen in this work as this fraction was proved to be the optimal ratio in the previous studies of ZrB_2-SiC and HfB_2-SiC systems, aiming to improve the mechanical properties and oxidation resistance [14,19-21]. $(Hf_{0.2}Zr_{0.2}Mo_{0.2}Nb_{0.2}Ti_{0.2})B_2$-SiC and $(Hf_{0.2}Mo_{0.2}Ta_{0.2}Nb_{0.2}Ti_{0.2})B_2$-SiC derived from borothermal reduction are hereafter labelled as HSBR-1 and HSBR-2, respectively. Similarly, the HEB samples from boro/carbothermal reduction are designated as HSBCR-1 and HSBCR-2.

The density of the HEB-SiC specimens was measured according to Archimedes' principle. The theoretical density of the HEB ceramics and HEB-SiC ceramics was calculated by rule of mixture. The theoretical density values of $(Hf_{0.2}Zr_{0.2}Mo_{0.2}Nb_{0.2}Ti_{0.2})B_2$ and $(Hf_{0.2}Mo_{0.2}Ta_{0.2}Nb_{0.2}Ti_{0.2})B_2$ ceramics was calculated to be 7.30 g/cm^3 and 8.61 g/cm^3, respectively. The purity of the SPSed samples was examined by powder X-ray diffraction (XRD; Cu-Kα radiation, D8, Bruker Co., Germany) on powder samples obtained from the sintered HEB-SiC specimens, with the scanning step-size from 2θ = 20 ~ 90°set as 0.02° dwelling for 0.2 s at each step. The lattice parameters of the products were calculated using the GSAS software package [22]. The carbon contents of HEB powders were determined using a carbon/sulfur analyser (CS-2000; ELTRA, Geremany) and oxygen contents of HEB-SiC ceramics were determined using nitrogen/oxygen determinator (TC600; Leco Corporation, St. Joseph, MI, USA). The microstructure was examined by scanning electron microscopy (SEM; Nova NanoSEM430, FEI, Netherlands) equipped with energy dispersive X-ray spectra analysis (EDS; Quantax 200, Bruker Co.). The average grain size of the HEB phase in the SPSed HEB-SiC samples etched in an acid mixture (HF:HNO_3:H_2O=1:1:3) for 1 min at room temperature was estimated from SEM images by Image-J software [23]. Vickers' hardness ($Hv_{0.2}$) of the ceramics was measured using a Vickers' Hardness Tester (HVS-30Z, Shanghai Taiming Optical Instrument Co., Ltd, China) with the load of 200 gf for 15 seconds, with at least 10 indentation points per sample. HEB-SiC ceramic toughness was measured by the indentation method with the load of 10 kgf for 10 seconds (> 10 indentation points per sample) with the toughness value calculated accordingly [24].

3. Results And Discussion

The relative density (RD) of the specimen was measured to be 100.0±0.4% and 99.1±0.1% for HSBR-1 and HSBR-2, respectively, indicative of nearly full densification, as listed in Table 1. Contrasted with HEB ceramics without SiC phase (97.7% and 95.0% in the same composition without SiC in Ref. [11], 98.1% and 98.5% in Ref. [12]), the densification of HEB ceramic material was improved by the introduction of SiC. Close values of RD were determined for the HSBCR series samples from boro/carbothermal reduction, suggesting that there was no obvious difference regarding the densification response between processing methods of borothermal reduction and boro/carbothermal reduction.

Table 1 Summary of the results on high-entropy boride-SiC ceramics in comparison with the reported results [4,11,12].

Composition	a (Å)	c (Å)	HE phase grain size (μm)	Relative density (%)	H*v* (GPa)	K_{IC} (MPa·m$^{1/2}$)
HSBR-1: $(Hf_{0.2}Zr_{0.2}Mo_{0.2}Nb_{0.2}Ti_{0.2})B_2$-20vol% SiC	3.0981	3.3645	3.99±0.73	100.0±0.4	25.8±1.2	4.53±0.66
HSBR-2: $(Hf_{0.2}Mo_{0.2}Ta_{0.2}Nb_{0.2}Ti_{0.2})B_2$-20vol% SiC	3.0812	3.3059	4.18±0.96	99.1±0.1	26.2±1.8	4.41±0.21
HSBCR-1: $(Hf_{0.2}Zr_{0.2}Mo_{0.2}Nb_{0.2}Ti_{0.2})B_2$-20vol% SiC	3.0980	3.3696	3.00±0.57	98.6±0.2	29.0±1.3	3.80±0.33
HSBCR-2: $(Hf_{0.2}Mo_{0.2}Ta_{0.2}Nb_{0.2}Ti_{0.2})B_2$-20vol% SiC	3.0875	3.3058	3.75±0.89	100.0±0.5	28.1±0.9	4.25±0.37
$(Hf_{0.2}Zr_{0.2}Mo_{0.2}Nb_{0.2}Ti_{0.2})B_2$[11]	3.0934	3.3526	*	97.7	26.3±0.7	*
$(Hf_{0.2}Mo_{0.2}Ta_{0.2}Nb_{0.2}Ti_{0.2})B_2$[11]	3.0820	3.3065	*	95.0	25.9±1.1	*
$(Hf_{0.2}Zr_{0.2}Mo_{0.2}Nb_{0.2}Ti_{0.2})B_2$[12]	3.0945	3.3592	1.45	98.1	26.3±1.8	*
$(Hf_{0.2}Mo_{0.2}Ta_{0.2}Nb_{0.2}Ti_{0.2})B_2$[12]	3.0821	3.2810	1.86	98.5	27.0±0.4	*
$(Hf_{0.2}Zr_{0.2}Mo_{0.2}Nb_{0.2}Ti_{0.2})B_2$ [4]	3.092	3.345	*	92.3	21.9±1.7	*
$(Hf_{0.2}Mo_{0.2}Ta_{0.2}Nb_{0.2}Ti_{0.2})B_2$ [4]	3.082	3.279	*	92.2	22.5±1.7	*

Powder XRD patterns of the HEB-SiC ceramics after SPS at 2000^{o}C are provided in Figure 1A. Characteristic peaks of a high-entropy boride phase were identified (space group of *P6/mmm*). In comparison with ZrB_2 and HfB_2 (as demonstrated in Figure 1, JCPDS PDF no. 65-8704 for ZrO_2 and PDF 65-8678 for HfO_2), the peaks of HEB phase shifted to the higher *2θ* range, indicative of the formation of a smaller crystal cell. Meanwhile, the reflections of α-SiC were detected at *2θ* = 34.1^o and 35.6^o (as shown in Figure 1B) and the peak intensities were weaker than those of HEB ceramic phase. In addition, the contamination of the oxide impurity (HfO_2) was observed in the HEB-SiC ceramics, similar to our previously reported studies [11,12]. It should be noted that the intensity of HfO_2 peaks in the product prepared by boro/carbothermal reduction were weaker than those by borothermal reduction. The oxygen contents in the as-obtained HEB-SiC ceramics were 2.08±0.01 wt.% in HSBR-1, 2.46±0.02 wt.% in HSBR-2, 1.86±0.04 wt.% in HSBCR-1, and 2.29±0.01 wt.% in HSBCR-2, respectively. The residual carbon content was evident for the products from boro/carbothermal reduction: 2.57 wt.% in $(Hf_{0.2}Zr_{0.2}Mo_{0.2}Nb_{0.2}Ti_{0.2})B_2$ and 1.65 wt.% in $(Hf_{0.2}Mo_{0.2}Ta_{0.2}Nb_{0.2}Ti_{0.2})B_2$, which was expected to react with the oxide impurities *via* carbothermal reduction reactions at high sintering temperature. The lattice parameters calculated by Rietveld refinement are also listed in Table 1. No obvious variations in lattice parameters were observed among the HEB phases prepared from borothermal reduction and boro/carbothermal reduction method.

EDS element mapping was employed to identify the impurity in HEB-SiC ceramics , shown in Figure 2. The grey phase observed as the matrix was high-entropy boride, and the dark-grey phase was SiC phase. According to the element mapping results (Figure 2), oxygen was detected in the white phase, which were identified as the oxide impurities indicated in the XRD results. Result of EDS mapping showed that the distribution of each element for each HEB-SiC ceramic was uniform. SiC phase exhibited homogeneous distribution in the HEB phase matrix with no agglomeration or solid solution with other elements from HEB.

The polished surface of the HEB-SiC ceramic after etching is shown in Figure 3. Observations showed that SiC mainly located in triple grain junctions. The average grain size of HEB phase in the composition was measured to be 3.99±0.73 μm in HSBR-1, 4.18± 0.96 μm in HSBR-2, 3.00±0.57 μm in HSBCR-1, and 3.75±0.89 μm in HSBCR-2, respectively. In our previous study [12], HEB ceramics without SiC prepared from borothermal reduction showed a relatively finer microstructure and the average grain size was 1~2 μm (Table 1). The enhanced grain growth in the current HEB-SiC ceramics was apparent as compared with the HEB ceramics without SiC under the same sintering conditions. This was unexpected as SiC is typically considered to refine the microstructure of simple diboride ceramics (e.g. ZrB_2), by means of pinning effects [19]. Whereas, the opposite phenomenon was observed for both HEB-SiC products prepared by the two powder processing routes. This suggests that the introduction of SiC into the HEB ceramics may be accompanied by liquid phase sintering, as oxygen impurity in SiC (*e.g.* amorphous SiO_2 layer on SiC) can form a eutectic phase. A liquid phase could accelerate the diffusion rate of the species involved in the densification mechanisms (dissolution-diffusion-reprecipitation) [25], which further promotes the grain growth of the HEB phase. Further experiments are under investigation to explain the mechanism and this work may provide some guidance for microstructure tuning of the HEB materials.

The average particle size of the starting HEB compounds from either borothermal reduction and boro/carbothermal reduction are measured to be in the range of 0.3 ~ 0.6 μm [11,12]. The microstructure of the HEB-SiC ceramics derived from borothermal reduction were expected to be comparable to boro/carbothermal reduction. However, from the microstructure analysis, it should be noted that a relatively finer grain size of HEB phase was observed in the HSBCR-1 and HSBCR-2 samples from boro/carbothermal reduction. This indicates that the processing routes of HEB powder affect the microstructure of the final HEB-SiC ceramics. This microstructure difference could be attributed to the presence of oxygen impurity and/or possible liquid phase, which promoted the coarsening of the boride grains. However, carbon residues present during boro/carbothermal reduction could facilitate the removal of oxygen impurities by carbothermal reduction, hence the grain growth of HEB phase was suppressed during high temperature sintering [14,15]. In addition, finer SiC particles were also observed in the samples prepared by boro/carbothermal reduction due to the smaller grain size of HEB phase in HSBCR-1 and HSBCR-2. The isolated SiC particles also suppressed the mass transfer and the SiC grains growth by providing a longer diffusion path.

The fracture surfaces of HEB-SiC ceramics are shown in Figure 4. Microstructure observations exhibited few pores and dense morphology in all compositions. The grey phase observed was high-entropy boride and the dark-grey phase was SiC particles. All the sintered specimens showed a transgranular fracture on the HEB phase. However, intergranular fracture behaviour on SiC grain was evident. A clear grain-pull-out and intergranular fracture of some SiC grains were observed (Figure 4a and b), which was absent on the microstructures derived from boro/carbothermal reduction (Fig. 4c and d). This was likely caused by removal of oxygen impurity in boro/carbothermal reduction, as a consequence, the grain boundary was purified and the bonding between grains was strong, leading to the transgranular fracture.

Measurements of Vickers' hardness and fracture toughness of the HEB-SiC ceramics were provided in Table 1. The hardness values were 25.8±1.2 GPa and 26.2±1.8 GPa in HSBR-1 and HSBR-2, respectively. It was shown that SiC could improve the densification of HSBR system, but didn't enhance the hardness mainly due to the grain coarsening effects (as discussed above). It was noteworthy that Vickers' hardness of HEB-SiC derived from boro/carbothermal reduction showed the higher values of 29.0±1.3 GPa in HSBCR-1 and 28.1±0.9 GPa in HSBCR-2. This could be attributed to the refined microstructure of HEB-SiC resulting from boro/carbothermal reduction. The toughness values were 4.53±0.66 MPa·$m^{1/2}$ and 4.41±0.21 MPa·$m^{1/2}$ in HSBR-1 and HSBR-2, 3.80±0.33 MPa·$m^{1/2}$ and 4.25±0.37 MPa·$m^{1/2}$ in HSBCR-1 and HSBCR-2, respectively. The HEB ceramics from borothermal reduction showed slightly higher toughness values, due to grain pull-out effect of some SiC grains (see Figure 4), which was assumed to deflect the crack propagation. The crack propagation of the HEB-SiC ceramics were observed by SEM, shown in Figure 5. Pronounced crack deflection and crack bridging was evidenced in the HEB-SiC samples derived from borothermal reduction, indicated by the white arrow in Figure 5a and b. Such crack deflection and bridging was believed to improve the toughness, attributed to the increasing path length for the crack fracture [13,14]. On the other hand, less crack deflection was apparent in HSBCR-1 and HSBCR-2 samples (Fig. 5c and d). Therefore, higher values of toughness in HSBR-1 and HSBR-2 were expected compared to HSBCR-1 and HSBCR-2.

It could be concluded that boro/carbothermal reduction route would not only refine the microstructure but also enhance the hardness of the final specimens. Meanwhile, the addition of SiC unexpectedly promoted the grain growth of high entropy boride phase in comparison with HEB ceramics without SiC. It was shown that the fracture toughness of HEB-SiC from borothermal reduction slightly increased with SiC addition. These findings provided a better understanding of processing route, the densification, and mechanical performance of high-entropy boride-silicon carbide ceramics. The results may inspire the further optimisation of both microstructure and mechanical properties of high-entropy boride-based materials for potential applications.

4. Conclusion

The processing routes of high-entropy boride powder via borothermal and boro/carbothermal reduction were examined and compared on $(Hf_{0.2}Zr_{0.2}Mo_{0.2}Nb_{0.2}Ti_{0.2})B_2$-SiC and $(Hf_{0.2}Mo_{0.2}Ta_{0.2}Nb_{0.2}Ti_{0.2})B_2$-SiC ceramics. The effects of SiC addition on the microstructure and the corresponding mechanical properties were also discussed. SiC was found to have little effect on the microstructure refinement. In comparison with those from borothermal reduction, the HEB-SiC ceramics from boro/carbothermal reduction exhibited the finer microstructure and thus relatively high Vickers' hardness values. The ultra-hard high-entropy boride-SiC ceramic, $(Hf_{0.2}Mo_{0.2}Ta_{0.2}Nb_{0.2}Ti_{0.2})B_2$-20 vol.% SiC, with a high hardness value of 29.0 GPa was obtained. Conversely, the intergranular fracture of some SiC grains was observed in the ceramics derived from borothermal reduction route, which led to the slight enhancement of fracture toughness. The current results indicate that the characteristics of the starting powders should also be considered when designing high-entropy boride-silicon carbide materials due to synergistic effects of processing route and secondary phase addition.

5. Declarations

Acknowledgements

This work was financially supported by State Key Laboratory for Modification of Chemical Fibers and Polymer Materials, Donghua University (No. 19ZK0113), the Pearl River S and T Nova Program of Guangzhou (No. 201710010142), Science and Technology Planning Project of Guangdong Province (No. 2017A050501033),

National Natural Science Foundation of China (No. 51402055, 51602060 and U1401247), and Guangdong Innovative and Entrepreneurial Research Team Program (Grant number No. 2013G061 and 2014YT02C049).

6. References

[1] Fahrenholtz WG, Hilmas GE, Talmy IG, *et al*. Refractory diborides of zirconium and hafnium. *J Am Ceram Soc* 2007, **90**:1347-1364.

[2] Liu D, Liu HH, Ning SS, *et al*. Chrysanthemum-like high-entropy diboride nanoflowers: A new class of high-entropy nanomaterials. *J Adv Ceram* 2020, **9**: 339-348.

[3] Liu D, Wen T, Ye B, *et al*. Synthesis of superfine high-entropy metal diboride powders. *Scripta Mater* 2019, **167**: 110-114.

[4] Gild J, Zhang Y, Harrington T, *et al*. High-entropy metal diborides: a new class of high-entropy materials and a new type of ultrahigh temperature ceramics. *Sci Rep* 2016, **6**: 37946.

[5] Tallarita G, Licheri R, Garroni S, *et al*. Novel processing route for the fabrication of bulk high-entropy metal diborides. *Scripta Mater* 2019, **158**: 100-104.

[6] Gu JF, Zou J, Sun SK, *et al*. Dense and pure high-entropy metal diboride ceramics sintered from self-synthesized powders via boro/carbothermal reduction approach. *Sci China Mater* 2019, **62**: 1-12.

[7] Zapata-Solvas E, Jayaseelan DD, Lin HT, *et al*. Mechanical properties of ZrB_2- and HfB_2-based ultra-high temperature ceramics fabricated by spark plasma sintering. *J Eur Ceram Soc* 2013, **33**: 1373-1386.

[8] Ni DW, Zhang GJ, Kan YM, *et al*. Hot pressed HfB_2 and HfB_2-20vol%SiC ceramics based on HfB_2 powder synthesized by borothermal reduction of HfO_2. *Int J Appl Ceram Technol* 2010, **7**: 830-836.

[9] Liu D, Wen T, Ye B*, et al*. Synthesis of superfine high-entropy metal diboride powders. *Scripta Mater* 2019, **167**: 110-114.

[10] Liu D, Liu H, Ning S*, et al*. Synthesis of high-purity high-entropy metal diboride powders by boro/carbothermal reduction. *J Am Ceram Soc* 2019, **102**: 7071-7076.

[11] Zhang Y, Guo WM, Jiang ZB, *et al*. Dense high-entropy boride ceramics with ultra-high hardness. *Scripta Mater* 2019, **164**: 135-139.

[12] Zhang Y, Jiang ZB, Sun SK, *et al*. Microstructure and mechanical properties of high-entropy borides derived from boro/carbothermal reduction. *J Eur Ceram Soc* 2019, **39**: 3920-3924.

[13] Buyakova SP, Knyazeva AG, Burlachenko AG, *et al*. Mechanical treatment of ZrB_2-SiC powders and sintered ceramic composites properties. *Res Develop* 2018, **1**: 521-530.

[14] Liu JX, Zhang GJ, Xu FF, *et al*. Densification, microstructure evolution and mechanical properties of WC doped HfB_2-SiC ceramics. *J Eur Ceram Soc* 2015, **35**: 2707-2714.

[15] Zou J, Zhang GJ, Vleugels J, *et al*. High temperature strength of hot pressed ZrB_2-20vol% SiC ceramics based on ZrB_2 starting powders prepared by different carbo/boro-thermal reduction routes. *J Eur Ceram Soc* 2013, **33**: 1609-1614.

[16]Zhang HZ, Hedman D, Feng PZ, *et al*. A high-entropy $B_4(HfMo_2TaTi)C$ and SiC ceramic Composite. *Dalton Trans* 2019, **48**: 5161-5167.

[17] Shen XQ, Liu JX, Li F, *et al*. Preparation and characterization of diboride-based high entropy $(Ti_{0.2}Zr_{0.2}Hf_{0.2}Nb_{0.2}Ta_{0.2})B_2$-SiC particulate composites. *Ceram Int* 2019, **45**: 24508-24514.

[18] Liu JX, Shen XQ, Wu Y, *et al*. Mechanical properties of hot-pressed high-entropy diboride-based ceramics. *J Adv Ceram* 2020, in press, https://doi.org/10.1007/s40145-020-0383-8.

[19] Guo WM, Zhang GJ, Wang PL. Microstructural evolution and grain growth kinetics in ZrB_2-SiC composites during heat treatment. *J Am Ceram Soc* 2009, **92**: 2780-2783.

[20] Mallik M, Kailath AJ, Ray KK, *et al*. Effect of SiC content on electrical, thermal and ablative properties of pressureless sintered ZrB_2-based ultrahigh temperature ceramic composites. *J Eur Ceram Soc* 2016, **37**: 559-572.

[21] Baharvandi HR, Mashayekh S. Effects of SiC content on the densification, microstructure, and mechanical properties of HfB_2-SiC composites. *Int J Appl Ceram Technol* 2020, **17**: 449-458.

[22] Toby BH. EXPGUI, a graphical user interface for GSAS. *J Appl Cryst* 2001, **34**: 210-213.

[23] Rueden CT, Schindelin J, Hiner MC, *et al*. ImageJ2: ImageJ for the next generation of scientific image data. *BMC Bioinf* 2017, **18**:529.

[25] Frederic M, Stefano G, Alida B. Advances in microstructure and mechanical properties of zirconium diboride based ceramics. *Mater Sci Eng A* 2003, **346**:310-319.

[1] Fahrenholtz WG, Hilmas GE, Talmy IG, *et al*. Refractory diborides of zirconium and hafnium. *J Am Ceram Soc* 2007, **90**:1347-1364.

[2] Liu D, Liu HH, Ning SS, *et al*. Chrysanthemum-like high-entropy diboride nanoflowers: A new class of high-entropy nanomaterials. *J Adv Ceram* 2020, **9**: 339-348.

[3] Liu D, Wen T, Ye B, *et al*. Synthesis of superfine high-entropy metal diboride powders. *Scripta Mater* 2019, **167**: 110-114.

[4] Gild J, Zhang Y, Harrington T, *et al*. High-entropy metal diborides: a new class of high-entropy materials and a new type of ultrahigh temperature ceramics. *Sci Rep* 2016, **6**: 37946.

[5] Tallarita G, Licheri R, Garroni S, *et al*. Novel processing route for the fabrication of bulk high-entropy metal diborides. *Scripta Mater* 2019, **158**: 100-104.

[6] Gu JF, Zou J, Sun SK, *et al*. Dense and pure high-entropy metal diboride ceramics sintered from self-synthesized powders via boro/carbothermal reduction approach. *Sci China Mater* 2019, **62**: 1-12.

[7] Zapata-Solvas E, Jayaseelan DD, Lin HT, *et al*. Mechanical properties of ZrB_2- and HfB_2-based ultra-high temperature ceramics fabricated by spark plasma sintering. *J Eur Ceram Soc* 2013, **33**: 1373-1386.

[8] Ni DW, Zhang GJ, Kan YM, *et al*. Hot pressed HfB_2 and HfB_2-20vol%SiC ceramics based on HfB_2 powder synthesized by borothermal reduction of HfO_2. *Int J Appl Ceram Technol* 2010, **7**: 830-836.

[9] Liu D, Wen T, Ye B*, et al*. Synthesis of superfine high-entropy metal diboride powders. *Scripta Mater* 2019, **167**: 110-114.

[10] Liu D, Liu H, Ning S*, et al*. Synthesis of high-purity high-entropy metal diboride powders by boro/carbothermal reduction. *J Am Ceram Soc* 2019, **102**: 7071-7076.

[11] Zhang Y, Guo WM, Jiang ZB, *et al*. Dense high-entropy boride ceramics with ultra-high hardness. *Scripta Mater* 2019, **164**: 135-139.

[12] Zhang Y, Jiang ZB, Sun SK, *et al*. Microstructure and mechanical properties of high-entropy borides derived from boro/carbothermal reduction. *J Eur Ceram Soc* 2019, **39**: 3920-3924.

[13] Buyakova SP, Knyazeva AG, Burlachenko AG, *et al*. Mechanical treatment of ZrB_2-SiC powders and sintered ceramic composites properties. *Res Develop* 2018, **1**: 521-530.

[14] Liu JX, Zhang GJ, Xu FF, *et al*. Densification, microstructure evolution and mechanical properties of WC doped HfB_2-SiC ceramics. *J Eur Ceram Soc* 2015, **35**: 2707-2714.

[15] Zou J, Zhang GJ, Vleugels J, *et al*. High temperature strength of hot pressed ZrB_2-20vol% SiC ceramics based on ZrB_2 starting powders prepared by different carbo/boro-thermal reduction routes. *J Eur Ceram Soc* 2013, **33**: 1609-1614.

[16]Zhang HZ, Hedman D, Feng PZ, *et al*. A high-entropy $B_4(HfMo_2TaTi)C$ and SiC ceramic Composite. *Dalton Trans* 2019, **48**: 5161-5167.

[17] Shen XQ, Liu JX, Li F, *et al*. Preparation and characterization of diboride-based high entropy $(Ti_{0.2}Zr_{0.2}Hf_{0.2}Nb_{0.2}Ta_{0.2})B_2$-SiC particulate composites. *Ceram Int* 2019, **45**: 24508-24514.

[18] Liu JX, Shen XQ, Wu Y, *et al*. Mechanical properties of hot-pressed high-entropy diboride-based ceramics. *J Adv Ceram* 2020, in press, https://doi.org/10.1007/s40145-020-0383-8.

[19] Guo WM, Zhang GJ, Wang PL. Microstructural evolution and grain growth kinetics in ZrB_2-SiC composites during heat treatment. *J Am Ceram Soc* 2009, **92**: 2780-2783.

[20] Mallik M, Kailath AJ, Ray KK, *et al*. Effect of SiC content on electrical, thermal and ablative properties of pressureless sintered ZrB_2-based ultrahigh temperature ceramic composites. *J Eur Ceram Soc* 2016, **37**: 559-572.

[21] Baharvandi HR, Mashayekh S. Effects of SiC content on the densification, microstructure, and mechanical properties of HfB_2-SiC composites. *Int J Appl Ceram Technol* 2020, **17**: 449-458.

[22] Toby BH. EXPGUI, a graphical user interface for GSAS. *J Appl Cryst* 2001, **34**: 210-213.

[23] Rueden CT, Schindelin J, Hiner MC, *et al*. ImageJ2: ImageJ for the next generation of scientific image data. *BMC Bioinf* 2017, **18**:529.

[25] Frederic M, Stefano G, Alida B. Advances in microstructure and mechanical properties of zirconium diboride based ceramics. *Mater Sci Eng A* 2003, **346**:310-319.

Figures

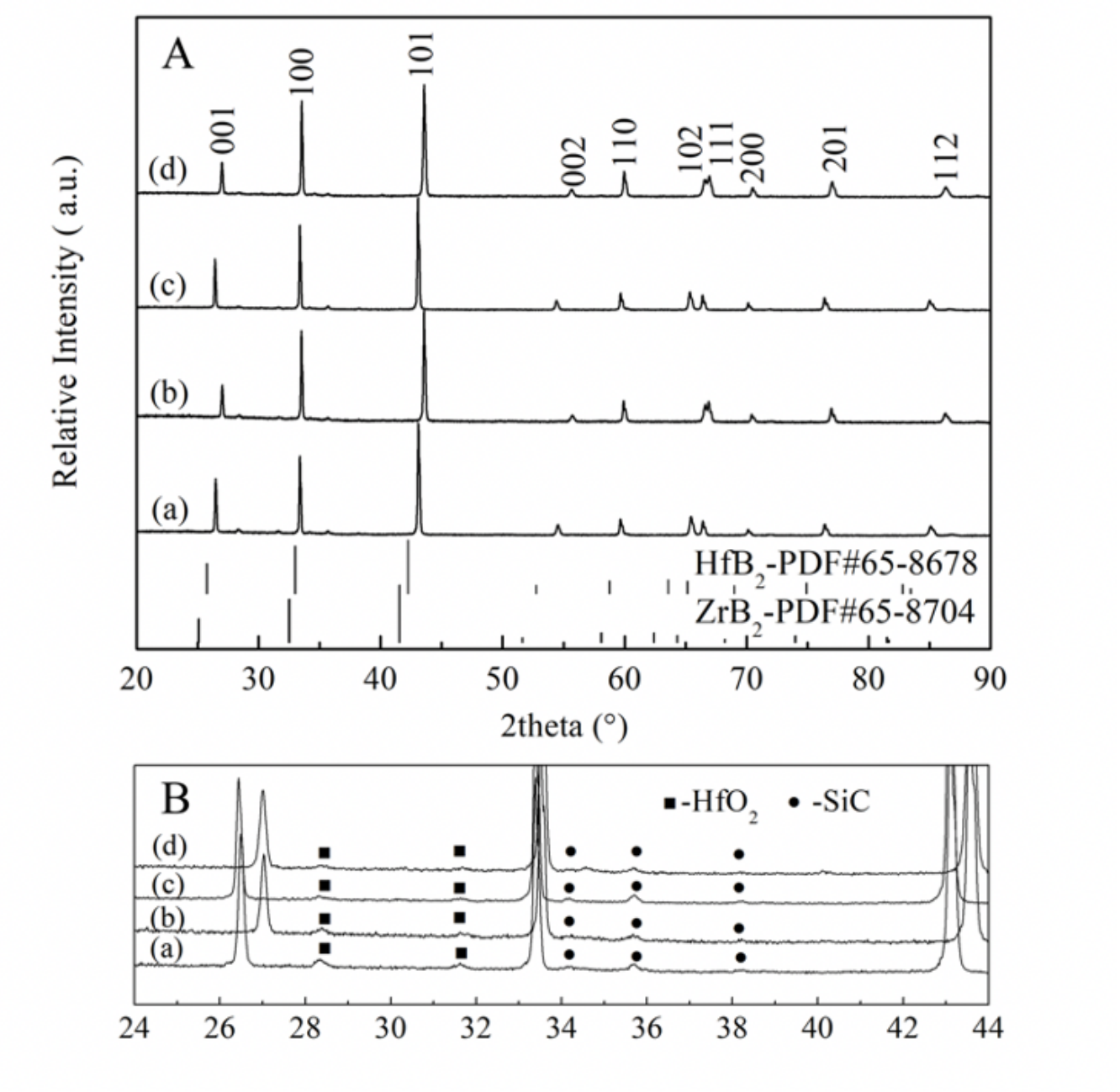

Figure 1

A. Powder XRD patterns of the HEB-SiC ceramics after SPS at 2000oC: a: HSBR-1, b: HSBR-2, c: HSBCR-1 and d: HSBCR-2. B. Enlarged view of the powder XRD patterns. The theoretical reflections of ZrB2 and HfB2 from JCPDS is

also displayed for comparison.

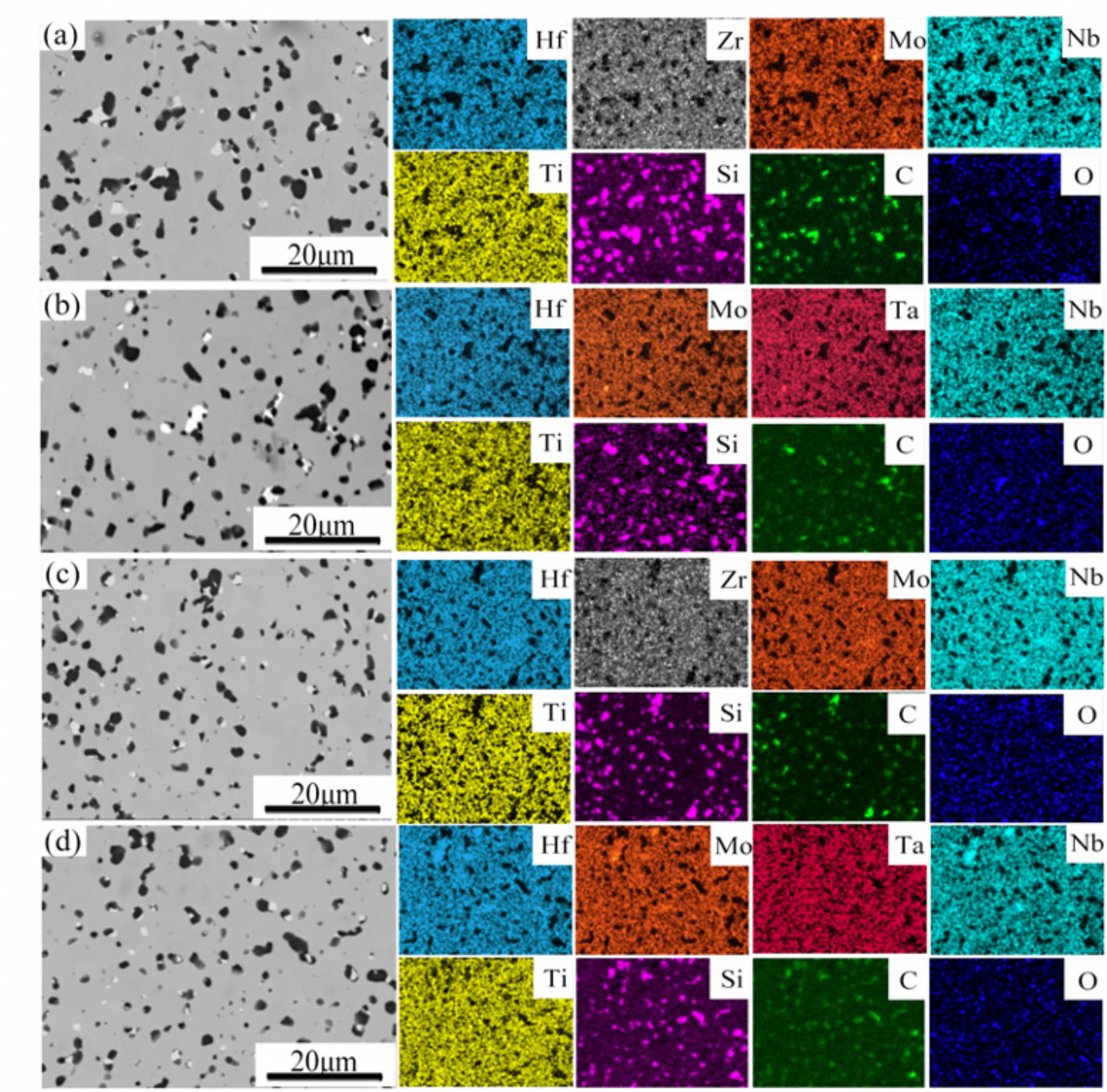

Figure 2

EDS mapping of HEB-SiC ceramics: a: HSBR-1, b: HSBR-2, c: HSBCR-1 and d: HSBCR-2.

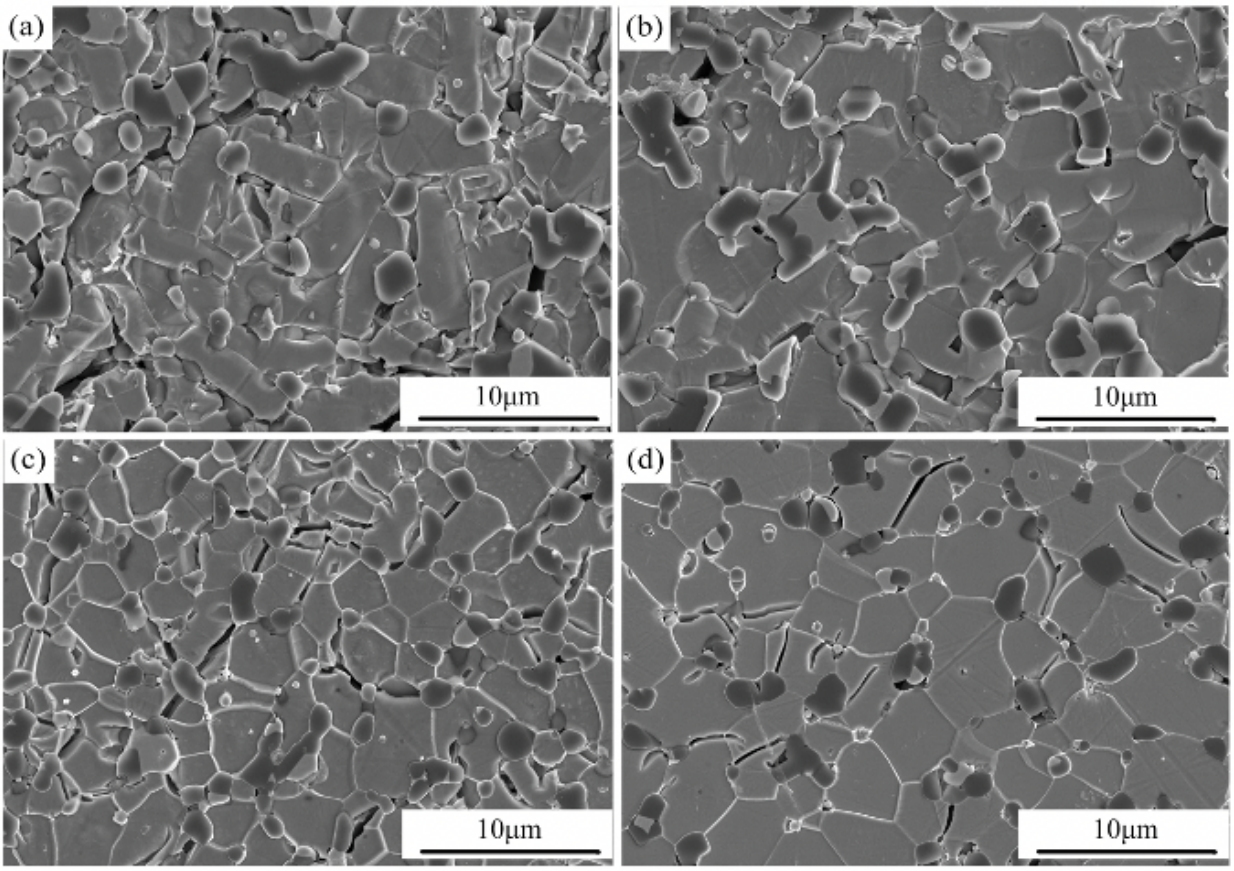

Figure 3

SEM images of the polished surface of the HEB-SiC ceramics after etching. a: HSBR-1, b: HSBR-2, c: HSBCR-1 and d: HSBCR-2.

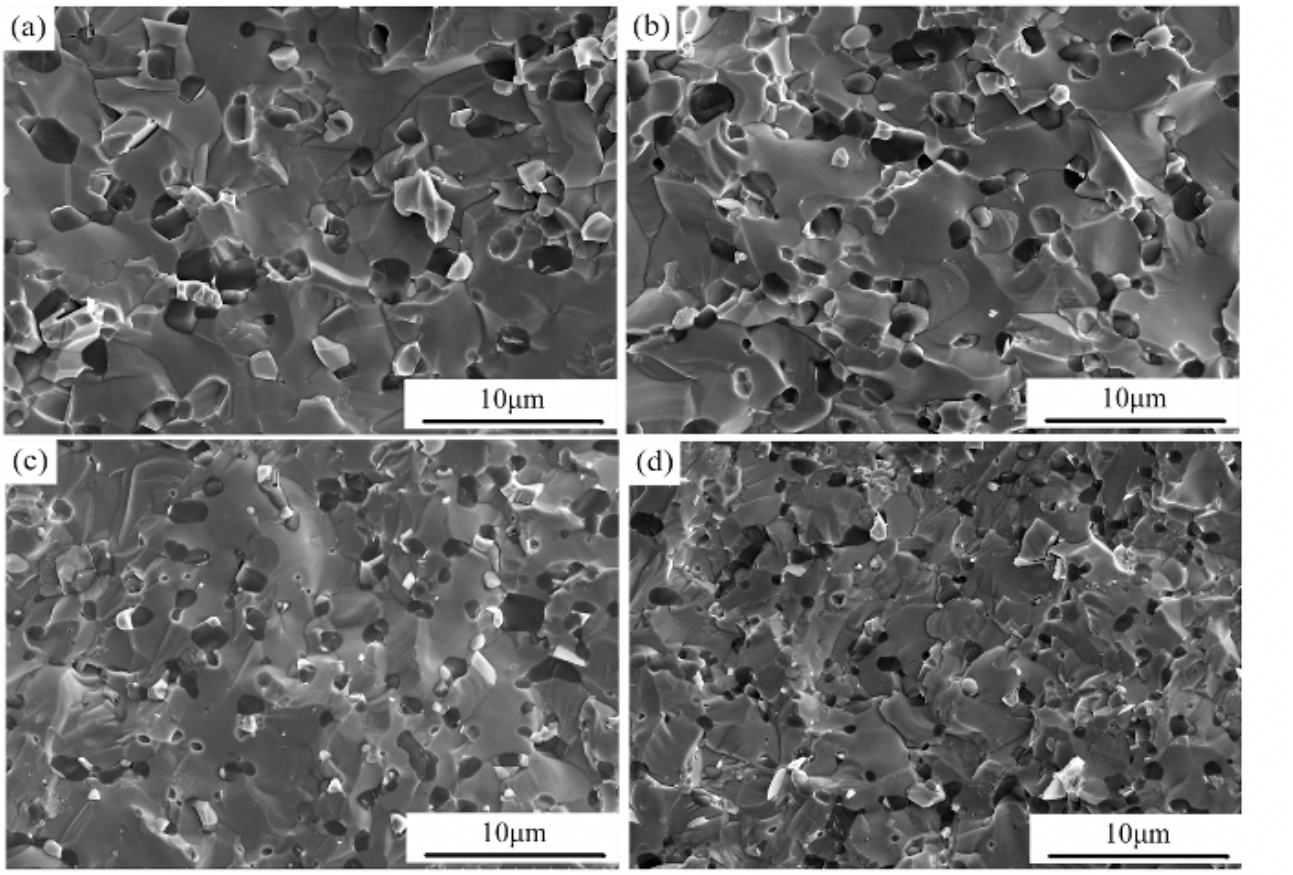

Figure 4

SEM images of the fracture surface of the HEB-SiC ceramics. a: HSBR-1, b: HSBR-2, c: HSBCR-1 and d: HSBCR-2.

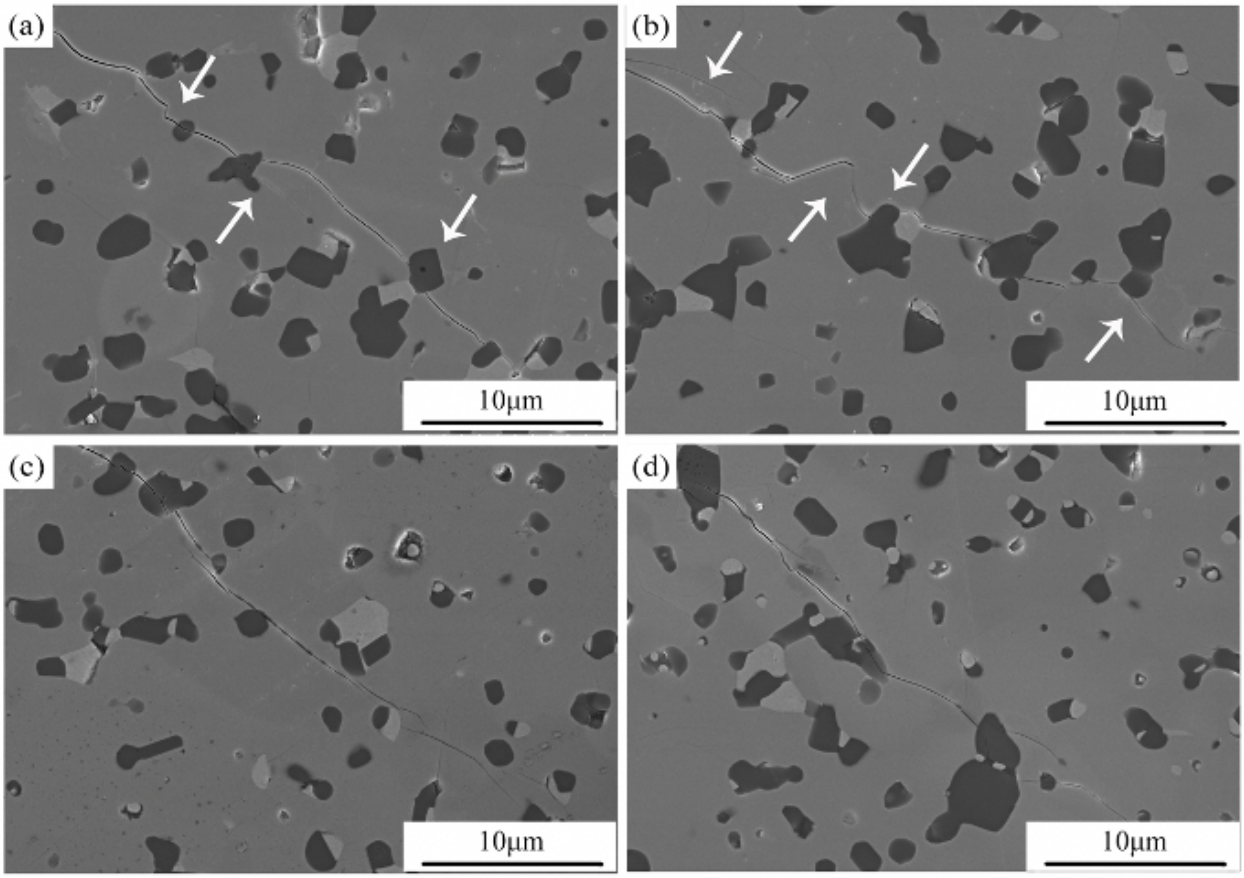

Figure 5

SEM images of the crack propagation of the HEB-SiC ceramics. a: HSBR-1, b: HSBR-2, c: HSBCR-1 and d: HSBCR-2.